

Available online at [www.sciencedirect.com](http://www.sciencedirect.com)

ScienceDirect

[www.journals.elsevier.com/journal-of-environmental-sciences](http://www.journals.elsevier.com/journal-of-environmental-sciences)JOURNAL OF  
ENVIRONMENTAL  
SCIENCES[www.jesc.ac.cn](http://www.jesc.ac.cn)

# Activated carbon coated palygorskite as adsorbent by activation and its adsorption for methylene blue

Xianlong Zhang<sup>1</sup>, Liping Cheng<sup>1</sup>, Xueping Wu<sup>1,\*</sup>, Yingzhao Tang<sup>1</sup>, Yucheng Wu<sup>2</sup>

1. School of Chemistry and Chemical Engineering, Hefei University of Technology, Hefei 230009, China.

E-mail: [zhangxianlong94@aliyun.com](mailto:zhangxianlong94@aliyun.com)

2. School of Materials Science and Engineering, Hefei University of Technology, Hefei 230009, China

## ARTICLE INFO

### Article history:

Received 23 September 2014

Revised 20 December 2014

Accepted 8 January 2015

Available online 2 May 2015

### Keywords:

Palygorskite/carbon

Activation

Adsorption

Methylene blue

Compressive strength

## ABSTRACT

An activation process for developing the surface and porous structure of palygorskite/carbon (PG/C) nanocomposite using  $ZnCl_2$  as activating agent was investigated. The obtained activated PG/C was characterized by X-ray diffraction (XRD), Fourier transform infrared spectroscopy (FTIR), field-emission scanning electron microscopy (SEM), and Brunauer–Emmett–Teller analysis (BET) techniques. The effects of activation conditions were examined, including activation temperature and impregnation ratio. With increased temperature and impregnation ratio, the collapse of the palygorskite crystal structure was found to accelerate and the carbon coated on the surface underwent further carbonization. XRD and SEM data confirmed that the palygorskite structure was destroyed and the carbon structure was developed during activation. The presence of the characteristic absorption peaks of C=C and C–H vibrations in the FTIR spectra suggested the occurrence of aromatization. The BET surface area improved by more than 11-fold ( $1201 \text{ m}^2/\text{g}$  for activated PG/C vs.  $106 \text{ m}^2/\text{g}$  for PG/C) after activation, and the material appeared to be mainly microporous. The maximum adsorption capacity of methylene blue onto the activated PG/C reached  $351 \text{ mg/g}$ . The activated PG/C demonstrated better compressive strength than activated carbon without palygorskite clay.

© 2015 The Research Center for Eco-Environmental Sciences, Chinese Academy of Sciences.

Published by Elsevier B.V.

## Introduction

Dyes are widely used in the chemical industry, and ever-increasing industrial applications of organic dye compounds have resulted in significant pollution of effluent waters and other environmental hazards (Benadjemia et al., 2011). These dyes are also harmful to humans with prolonged contact. Methylene blue (MB), a common pollutant in dye effluents, is difficult to remove completely because of its stable aromatic structure consisting of a chromophore and polar groups (Liu et al., 2012). Various techniques have been developed to improve the efficiency of MB removal, including adsorption, chemical oxidation, and electro-coagulation. Among these, adsorption

has proven particularly effective, mainly because of its simplicity and efficiency.

Activated carbon works as an excellent adsorbent for the removal of most organic contaminants because of its high surface area and wide porosity. Activated carbon can be produced by physical or chemical activation using various carbonaceous materials (Mohanty et al., 2005; Juang et al., 2000; Theydan and Ahmed, 2012; Zhu et al., 2007; Khezami et al., 2005; Yue et al., 2013). Compared to physical activation, chemical activation can confer particular surface and pore characteristics to activated carbon through the use of various biomass materials as precursors, including lignin, peat, and leaves (Hayashi et al., 2000; Chiu and Ng, 2012; Donald et al.,

\* Corresponding author. E-mail: [xuepingw@ustc.edu.cn](mailto:xuepingw@ustc.edu.cn) (Xueping Wu).

2011; Saka, 2012; Altenor et al., 2009). Furthermore, development of the pore structures can be easily adjusted by changing activation conditions such as temperature, impregnation ratio, and activating agents (Williams and Reed, 2006; Uçar et al., 2009; Nakagawa et al., 2007; Yavuz et al., 2010). Reffas et al. (2010) prepared activated carbon with a total surface area of 925 m<sup>2</sup>/g from coffee grounds using H<sub>3</sub>PO<sub>4</sub> as the activating agent. Chiu and Ng (2012) synthesized activated carbon fiber with Brunauer–Emmett–Teller (BET) surface area of 2060 m<sup>2</sup>/g from cotton using ZnCl<sub>2</sub>. The demand for activated carbon is growing rapidly because of increasing industrial pollution; however, high price has limited its application.

Palygorskite (PG) is a type of magnesium aluminum silicate mineral that exists widely in nature. In our previous study, a novel palygorskite/carbon (PG/C) sorbent was prepared by hydrothermal carbonization of glucose or cellulose using palygorskite as template (Wu et al., 2011, 2014a,b). Given the combination of the crystal structure of PG and the organophilic nature of carbon, PG/C has high adsorption capacity for some typical organic pollutants, such as MB and phenol. PG/C offers advantages such as its inexpensive raw materials, low cost, and green production. However, its specific surface area is rather low compared to that of activated carbon.

This study focused on the activation process of PG/C nanocomposite and aimed to produce activated samples with high surface area and porosity. Previous studies have showed that porous carbon with more stable performance can be obtained by hydrothermal methods (Hao et al., 2013; Wang et al., 2011; Regmi et al., 2012; Ding et al., 2013; Román et al., 2013). Román et al. (2013) prepared adsorbents from biomass by combining hydrothermal carbonization and activation. The hydrothermal carbons produced in this manner presented low BET surface areas of only about 30 m<sup>2</sup>/g, which increased up to 438 m<sup>2</sup>/g after CO<sub>2</sub> activation. It was reported that the initial hydrothermal treatment step allowed better control over the resulting porosity and that the activation step was crucial in the development of porosity in hydrothermal carbons. Furthermore, this method offered the ability to change surface functionalities and improved the final yield of the subsequent activation process. In the current study, the previously studied PG/C nanocomposite was further activated to develop a carbon pore structure coated onto PG. The influences of ZnCl<sub>2</sub> impregnation ratio and activation temperature on surface characteristics were then investigated. In addition, adsorption of MB onto the activated samples prepared under different conditions was compared.

## 1. Materials and methods

### 1.1. Raw materials

PG raw material was acquired from Jiangsu Province, China and sieved to 200 mesh. The chemical composition and texture properties were determined by chemical analysis and X-ray diffraction. The chemical composition of the clay was 57.01% SiO<sub>2</sub>, 8.78% Al<sub>2</sub>O<sub>3</sub>, 12.82% MgO, 4.28% Fe<sub>2</sub>O<sub>3</sub>, 0.08% FeO, and 17.03% others. All reagents (cellulose, ammonium iron sulfate hexahydrate (FeSO<sub>4</sub>(NH<sub>4</sub>)<sub>2</sub>SO<sub>4</sub>·6H<sub>2</sub>O), hydrochloric acid (HCl), hydrofluoric acid (HF), anhydrous zinc chloride

(ZnCl<sub>2</sub>), and methylene blue (MB)) were of analytical grade and were bought from Sinopharm Group Co., Ltd (Shanghai, China) and used as received without further purification. Commercial activated carbon was obtained from the Institute of Coal Chemistry, Chinese Academy of Sciences. Only double-distilled water was used.

### 1.2. Preparation of palygorskite/carbon (PG/C) nanocomposite

The PG/C sample was prepared based on a previously reported method (Wu et al., 2011, 2014a,b). Cellulose (5 g) and FeSO<sub>4</sub>(NH<sub>4</sub>)<sub>2</sub>SO<sub>4</sub>·6H<sub>2</sub>O (2.80 g) were dissolved in 72 mL double-distilled water. PG (2.5 g) was then added and the mixture was stirred for 2 hr at room temperature. The final suspension was transferred to a Teflon-lined stainless-steel autoclave (100 mL in total inner volume), sealed, and maintained at 220°C for 12 hr. The black product was centrifuged, washed with double-distilled water and ethanol several times, and then dried in an oven at 105°C for 8 hr.

### 1.3. Activation

The dried PG/C nanocomposites were passed through a 200-mesh sieve prior to chemical activation with ZnCl<sub>2</sub>. Appropriate amounts of PG/C powder and anhydrous ZnCl<sub>2</sub> were dispersed in water to obtain the desired impregnation mass ratio ZnCl<sub>2</sub>:PG/C composites. To remove moisture after impregnation, the samples were dried for 24 hr at 105°C in an oven and then heated for another hour at various temperatures under a controlled heating rate of 5°C/min and nitrogen atmosphere. To remove any residual organic and mineral matter, the sintered samples were washed with 1.2 mol/L HCl solution and then rinsed with hot distilled water until the pH value reached 7. Lastly, the samples were dried at 105°C.

The activation temperature was set at 450°C for experiments investigating the effect of varying impregnation ratios, whereas, the impregnation ratio was set at 1:1 for the experiments investigating the effect of varying activation temperatures. The samples were labeled as PG/C-Ax-y/z, where x stands for activation temperature, and y/z for impregnation weight ratio of ZnCl<sub>2</sub> and PG/C composites. The PG clay in the activated PG/C was removed by washing the composite in 40 wt.% HF solution at room temperature for 20 hr followed by several rounds of washing with double-distilled water and, lastly, drying at 105°C.

### 1.4. Characterization

Power X-ray diffraction analysis (XRD) was performed using an X-ray diffractometer with Cu anode operating at 40 kV and 100 mA (D/MAX2500V, Rigaku, Japan). Elemental analysis (EA) was conducted on an elemental analyzer (Vario EL c, Elementar, Germany). Thermal analysis (DSC-TG) curves of PG were recorded with a simultaneous thermal analyzer (Q2000, TA, USA). The sample was heated from room temperature to 700°C at 10°C/min under N<sub>2</sub> flow. Fourier transform infrared spectra of the samples were obtained in the range of 4000–400 cm<sup>-1</sup> in a FTIR spectrometer (Thermo, Madison, USA) using KBr pellets. The morphology and particle size of the products were observed with a field-emission scanning electron microscope (SEM, JSM-6700, JEOL, Japan). Brunauer–Emmett–Teller (BET) analysis

was conducted with a specific area and pore analyzer (TriStar II 3020, Micromeritics, USA). Compressive strength was measured using a dynamic mechanical analyzer (DMA) testing machine (Q800, TA, USA). The test temperature was set at 25°C and the ramp force was increased at a rate of 0.5 kg-m/(sec<sup>2</sup>-min) to 18.0 kg-m/sec<sup>2</sup>.

### 1.5. Adsorption of methylene blue (MB)

Adsorption studies were carried out with 20 mg activated samples that were introduced into a 50 mL MB solution at an initial concentration of 100 mg/L. The pH values of the suspensions were not adjusted. The adsorption equilibrium of MB on the prepared materials was obtained after 24 hr of shaking at 25°C and 200 r/min. After centrifugation and filtration, the MB equilibrium concentrations were determined from the absorbance of the samples at 665 nm using a visible spectrophotometer (722E, Shanghai Spectrum Co., Ltd., China).

The removal rate of MB ( $\eta$ , %) was calculated using the equation below.

$$\eta (\%) = \frac{c_0 - c_e}{c_0} \times 100\% \quad (1)$$

$$q_e = \frac{(c_0 - c_e)V}{m} \quad (2)$$

where,  $c_0$  (mg/L) and  $c_e$  (mg/L) are the initial and equilibrium MB concentrations, respectively;  $q_e$  (mg/g) is the adsorption capacity at equilibrium,  $V$  (L) is the volume of solution and  $m$  (g) is the dosage of the adsorbent.

To evaluate the adsorption capacity of the activated samples, different initial concentrations (10–300 mg/L) of MB solutions were prepared. Adsorption isotherms of MB were fitted to the Langmuir model using the following linearized Langmuir equation:

$$\frac{c_e}{q_e} = \frac{1}{bq_m} + \frac{c_e}{q_m} \quad (3)$$

where  $b$  (L/mg) is the Langmuir constant, and  $q_m$  (mg/g) is the maximum amount of MB.

## 2. Results and discussion

### 2.1. Product yield

Table 1 lists the product yields after activation. Product yields of the activated samples ranged from 35% to 40%. Compared

to the reported yields of activated carbon (Romero-Anaya et al., 2014), the yield values obtained in this study were higher, which was attributed to the small weight loss of PG clay during activation.

### 2.2. XRD data

Fig. 1a shows the typical XRD patterns of the composite precursor and activated products at different ZnCl<sub>2</sub> impregnation ratios. According to the XRD data, the diffraction peaks at  $2\theta = 8.3^\circ$ ,  $13.6^\circ$ ,  $19.8^\circ$ , and  $27.3^\circ$  could be attributed to the characteristic diffraction peaks of PG (Wu et al., 2011, 2014a,b). The peak at  $2\theta = 26.7^\circ$  corresponded to a low content quartz impurity (Banaš et al., 2013). In the case of activated products, the highest intensity of PG at  $2\theta = 8.3^\circ$  decreased gradually and simultaneously a broad and weak peak due to the amorphous carbon appeared between  $2\theta = 20^\circ$  to  $30^\circ$  (Liu et al., 2013) with increasing impregnation ratios. This may be due to the possibility that ZnCl<sub>2</sub> at high concentration could have encroached into the internal channels previously formed in the PG/C composite, which causes the crystal structure of the composite to fold further after increasing the amount of the activating agent. The carbon coated on the PG surface was activated and the pore structure was developed, resulting in the appearance of a carbon reflection in the activated samples. When the impregnation ratio reached 2:1, the characteristic peak of PG almost disappeared. The yield and carbon content of the activated product decreased with increasing ZnCl<sub>2</sub> impregnation amount (Table 1), implying that higher carbon loss occurred during activation and carbonization. The outer carbon played a role in protecting the inner PG from heating destruction. Consequently, the inner PG gradually lost the protection of the outer carbon and the destruction of its crystal structure was accelerated at increasing impregnation ratios.

Activation temperature also plays an important role in the activation process. As shown in Fig. 1b, the crystal structure of activated samples changed with the activation temperature. As the activation temperature increased from 450°C to 550°C, the characteristic peaks of PG at  $2\theta = 8.3^\circ$ ,  $13.6^\circ$ ,  $19.8^\circ$ , and  $27.3^\circ$  decreased. Fig. S1 shows the DSC-TG analysis curves of PG. The zeolitic water (Kuang et al., 2004) was released in the temperature range from 40°C to 117°C. The first and second structural water (Kuang et al., 2004) were released at 130°C–230°C and 230°C–470°C, respectively. Dehydroxylation of the Mg–OH groups (Kuang et al., 2004; Frost and Ding, 2003) occurred at 470°C–633°C. The DSC-TG curves indicated that the release of the second structural water and dehydroxylation of the Mg–OH groups occurred during activation in the

**Table 1 – Elemental content and yield of activated samples.**

Sample	C (wt.%)	H (wt.%)	N (wt.%)	S (wt.%)	Yield (wt.%)
PG/C-A450-1/2	42.19	2.22	2.60	0.35	40
PG/C-A450-1/1	38.74	2.63	3.18	0.25	37
PG/C-A450-2/1	36.61	2.68	2.79	0.24	36
PG/C-A500-1/1	37.78	3.08	3.81	0.25	36
PG/C-A550-1/1	35.44	2.48	3.11	0.29	35

PG/C-A450-1/2, PG/C-A450-1/1, PG/C-A450-2/1, PG/C-A500-1/1, and PG/C-A550-1/1 refer to Section 1.3.

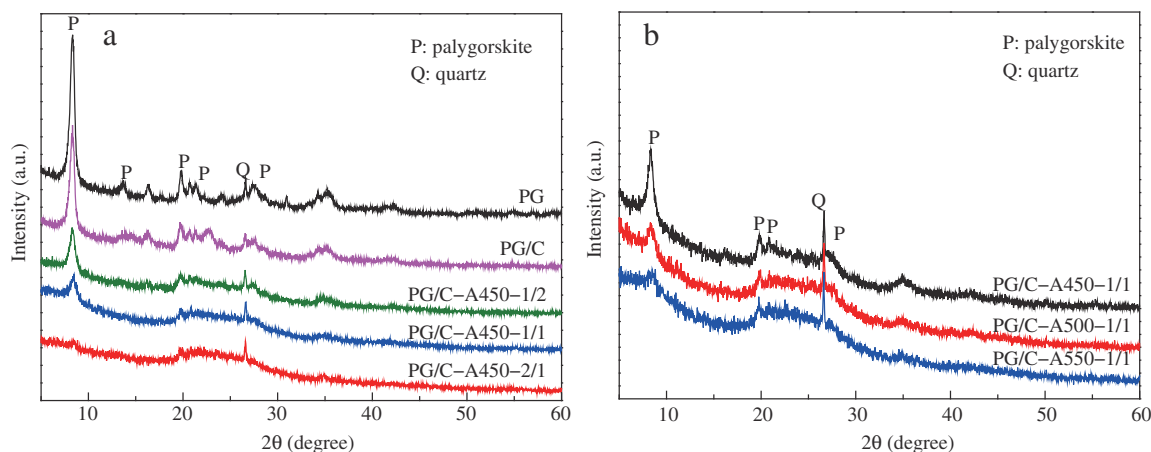


**Fig. 1** – XRD patterns of palygorskite (PG), palygorskite/carbon (PG/C) and activated samples at different  $\text{ZnCl}_2$  impregnation ratios (a) and different activation temperatures (b). PG/C-A450-1/2, PG/C-A450-1/1, PG/C-A450-2/1, PG/C-A500-1/1, and PG/C-A550-1/1 refer to Section 1.3.

temperature range of 450°C to 550°C, which resulted in the folding of the PG structure (Chen et al., 2011) and considerable decrease in the XRD patterns as shown in Fig. 1b.

### 2.3. SEM images

The SEM images of the PG/C and activated PG/C-A450-1/1 samples are shown in Fig. 2. In the case of PG/C, the PG fibers were evidently coated with a number of nanoparticles, namely nanocarbon particles, as previously reported (Wu et al., 2011, 2013). After activation, the collapse of PG fibers (Fig. 1b), which was brought about by heating and encroachment by  $\text{ZnCl}_2$ , directly resulted in the accumulation of PG nanofibers (Fig. 2b). The carbon coated on the PG surface further underwent carbonization during activation (Román et al., 2013) and remained compactly coated on the PG surface.

### 2.4. FTIR spectra

The FTIR spectra of different samples are shown in Fig. 3. In the case of PG/C, the bands at 3615 and 3557, as well as 3394  $\text{cm}^{-1}$  are due to hydroxyl groups or adsorbed water (Guo and Rockstraw, 2006). The band at 2914  $\text{cm}^{-1}$  is due to the C–H

stretching vibration (Wu et al., 2011). The band at 1654  $\text{cm}^{-1}$  is attributed to the bending vibrations of the adsorbed and zeolitic water in PG. The bands at 1383  $\text{cm}^{-1}$  and 793  $\text{cm}^{-1}$  are brought about by the C=O bending vibration in the carbonyl and aromatic C–H out-of-plane bending vibrations, respectively (Li et al., 2011). The band at 1197  $\text{cm}^{-1}$  is assigned to the stretching vibrations of (Mg, Al)–O bonds (Wu et al., 2011). After activation, the FTIR spectra of activated PG/C were markedly different from those of PG/C. The characteristic peaks of PG at 1654 and 1197  $\text{cm}^{-1}$  nearly disappeared, which resulted from the folding and subsequent collapse of the PG fiber structure (Figs. 1a and 2). The peaks assigned to amorphous carbon in PG/C at 2914 and 1383  $\text{cm}^{-1}$  also nearly disappeared. Simultaneously, a new band appeared at 1622  $\text{cm}^{-1}$ , which could be attributed to the C=C group, and the band at 793  $\text{cm}^{-1}$  became more intense, indicating that aromatization took place (Chang et al., 2014; Román et al., 2013; Li et al., 2011). As the impregnation ratio increased, the bands at 1622 and 793  $\text{cm}^{-1}$  became more intense and then slightly weakened. The intensities of the two bands were the strongest when PG/C was activated at 450°C under 1:1 impregnation ratio, implying that activation of the carbon coating was the most aggressive at this point.

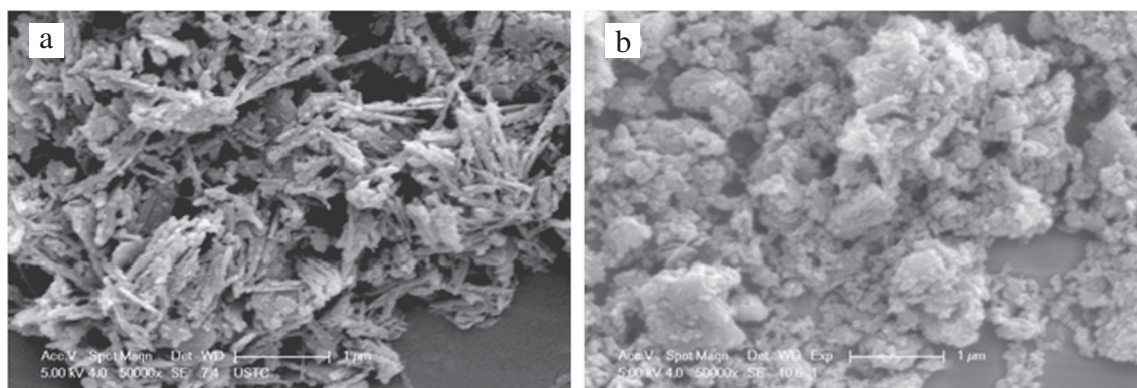


**Fig. 2** – SEM images of (a) palygorskite/carbon (PG/C) and (b) PG/C-A450-1/1.

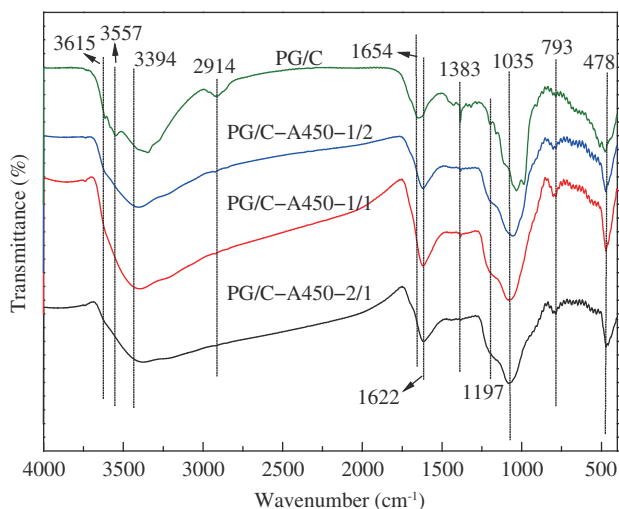


**Fig. 3 – FTIR spectra of palygorskite/carbon (PG/C) and activated samples at different ZnCl<sub>2</sub> impregnation ratios.**

**2.5. Surface area and pore structure**

Fig. 4a shows the effect of immersion ratio on the N<sub>2</sub> adsorption-desorption curves. The curve of PG/C indicates that the adsorption isotherm exhibits a type II shape based on IUPAC classification, representing unrestricted monolayer-multilayer adsorption (Sing et al., 1985). This implies that PG/C is a non-porous or macroporous adsorbent. As immersion ratio changed, an apparent change in the N<sub>2</sub> adsorption-desorption isotherms occurred. At 1:2 impregnation ratio, the curve acquired a typical type I shape. The adsorption and desorption curves of PG/C-A450-1/2 almost overlapped, implying the presence of a large amount of micropores (Reffas et al., 2010). N<sub>2</sub> uptake increased when the impregnation ratio increased from 1:2 to 1:1. In addition, the curve of PG/C-A450-1/1 showed a small hysteresis loop, suggesting the presence of mesopores. Nevertheless, the isotherm of PG/C-A450-2/1 displayed a combination of type I and IV shape with pronounced H4-type hysteresis loop (Miao et al., 2013), which suggests that more mesopores appeared when the amount of activation agent was

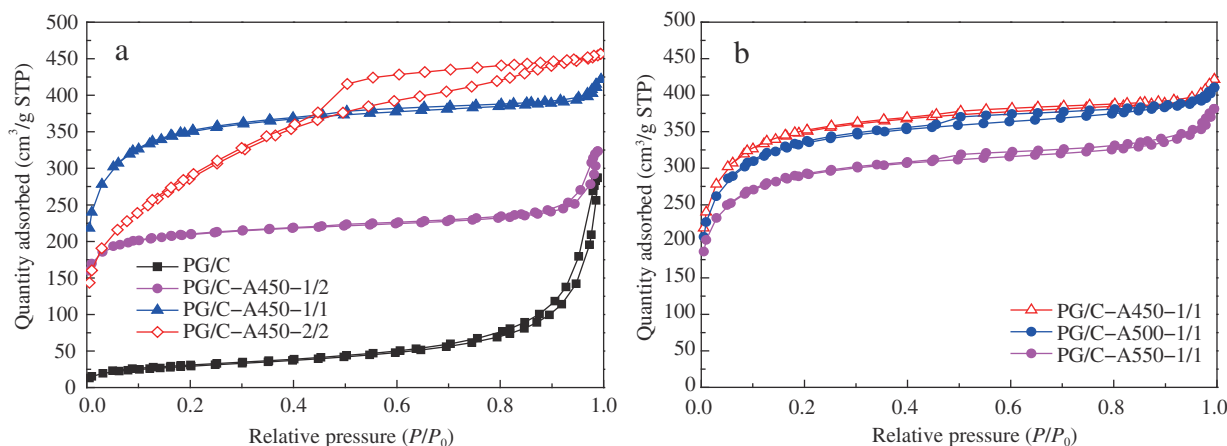
increased further. As observed in Table 2, the micropore area decreased sharply as ZnCl<sub>2</sub> and composite ratio increased to 2:1. With an increase in impregnation ratio, micropore content decreased and larger pores were produced, which eventually led to lower surface area. The relevant surface area data are shown in Table 2. Notably, the BET surface area of PG/C significantly increased from 106 to 1201 m<sup>2</sup>/g after activation.

Fig. 4b shows the effect of activation temperature on N<sub>2</sub> adsorption-desorption isotherms. It was observed that activated PG/C samples obtained at different temperatures were microporous. The isotherms presented type I curves with small hysteresis loops (Sing et al., 1985). N<sub>2</sub> adsorption increased sharply at relatively low pressure and then reached a plateau at higher pressure, indicating that the materials were predominantly microporous (Sing et al., 1985). The small hysteresis loops suggest the presence of mesopores (Williams and Reed, 2006). N<sub>2</sub> adsorption decreased with increased activation temperature, indicating that higher temperature enhanced carbon burn out as carbonization progressed and also destroyed the crystal structure of the template, resulting in lower surface area. However, the type I shape of the isotherms was maintained, suggesting that the increase in activation temperature did not change the microporosity of the activated PG/C.

**2.6. Methylene blue (MB) adsorption**

Fig. 5a shows dynamic adsorption of MB with different initial concentrations on PG/C-A450-1/1. With prolonged contact time, the MB adsorption capacity (q<sub>t</sub>) increased gradually and then reached a plateau, indicating that the MB amount being adsorbed onto the adsorbent and desorbing from the adsorbent reached an equilibrium (Foo and Hameed, 2012). It took less time to reach equilibrium under low MB concentrations. Our data indicate that 24 hr was sufficient to reach equilibrium.

Fig. 5b shows the adsorption isotherms of MB on unactivated PG/C and activated PG/C. It is worth noting that PG/C-A450-2/1 showed better adsorption performance than PG/C-A450-1/1 with increasing initial concentration, although the former had higher BET surface area. The aggregation of MB at high concentration usually occurs in aqueous solution (Zhou et al.,



**Fig. 4 – N<sub>2</sub> adsorption-desorption isotherms at –196°C on unactivated palygorskite/carbon (PG/C) and activated samples at (a) different impregnation ratios and (b) different activated temperatures.**

**Table 2 – Textural characteristics obtained by N<sub>2</sub> adsorption–desorption analysis.**

Sample	BET surface area (m <sup>2</sup> /g)	Micropore area (m <sup>2</sup> /g)	External surface area (m <sup>2</sup> /g)	Total pore volume (cm <sup>3</sup> /g)	Micropore volume (cm <sup>3</sup> /g)
PG/C	106	5.7	100	0.3022	0.0012
PG/C-A450-1/2	709	526	183	0.4301	0.2438
PG/C-A450-1/1	1201	712	489	0.6157	0.3257
PG/C-A450-2/1	1044	38	1006	0.6960	0.0022
PG/C-A500-1/1	1151	630	521	0.6066	0.2874
PG/C-A550-1/1	1000	576	424	0.5466	0.2629

PG/C: palygorskite/carbon.

2014), with the result that MB was easier to adsorb on the external surface. Thus the highest adsorption capacity was achieved by PG/C-A450-2/1 because it had the highest external surface area and total pore volume (Table 2).

The maximum adsorption capacity ( $q_m$ ) values of MB calculated by Eq. (3) are shown in Table 3. Notably, the  $q_m$  value (351 mg/g) of MB onto the activated carbon-coated PG sample (PG/C-A450-2/1) was far higher than that of untreated PG/C (89 mg/g). This value was even higher than that of normal activated carbon (318 mg/g). After removing the PG template with HF acid, the  $q_m$  of MB onto the obtained activated carbon (AC) reached 337 mg/g. Thus, the carbon coated on the PG surface made a significant contribution to the adsorption of MB, leading to the relatively high  $q_m$  value compared to that of stripped AC.

The high  $q_m$  value (351 mg/g) of MB onto the activated carbon-coated PG sample (PG/C-A450-2/1) can be explained as follows. First, activated PG/C contains abundant functional groups including C=O, -OH and C=C on its surface. It was previously reported that acidic groups such as carboxyl, lactonic, hydroxyl and carbonyl groups favor MB adsorption (Altenor et al., 2009). Compared to untreated PG/C, it presents a more extensive pore structure and higher BET surface area (709–1201 m<sup>2</sup>/g). These factors are beneficial for the enhancement of adsorption capacity of MB. Second, MB is a cationic dye containing quaternary ammonium salt ( $[\text{C}_{16}\text{H}_{18}\text{N}_3\text{S}]^+\text{Cl}^-$ ), which is positively charged (Altenor et al., 2009). The PG/C adsorbent is negatively charged when the pH of the adsorption solution is not adjusted (Wu et al., 2014a,b). The molecular

dimension of MB is 1.63 nm × 0.56 nm × 0.54 nm (Chen et al., 2011), and it can easily be adsorbed on the external surface and pores that are larger than its molecular size. Thus, the excellent adsorption capacity of MB onto the activated PG/C was made possible due to its polarity and size.

## 2.7. Activation mechanism

To determine the activation mechanism, the structural changes and adsorption capacity of different samples were compared, as shown in Fig. 6 and Table 4. The XRD pattern of PG/C showed the typical peak characteristics of PG (Fig. 1), which were similar to those found in previous studies (Wu et al., 2011, 2013, 2014a,b). After heating the PG at 450°C for 1 hr (sample PG-450), the intensity of PG peaks weakened, implying destruction of the PG crystal structure. The PG was impregnated with ZnCl<sub>2</sub> at a weight ratio of 1:1 and then calcined at 450°C. This sample, labeled as PG-A450-1/1, was prepared to undergo activation. Similarly, the PG peaks almost disappeared and the new peaks at  $2\theta = 33^\circ$  and  $35.7^\circ$  were attributed to ZnO, which may be generated during the activation process and is not completely removed by washing (Zhao et al., 2012). The adsorption capacity of MB on PG-450 at equilibrium ( $q_e$ ) reached 70 mg/g and the removal rate of MB was 28%. These values of  $q_e$  and  $\eta$  for PG-450 suggested that heating of PG was not the main contributor to the observed increase in adsorption capacity of activated PG/C (PG/C-A450-1/1), which had  $q_e$  and  $\eta$  values of 220 mg/g and 87%, respectively. The  $q_e$  and  $\eta$  values for PG-A450-1/1 were

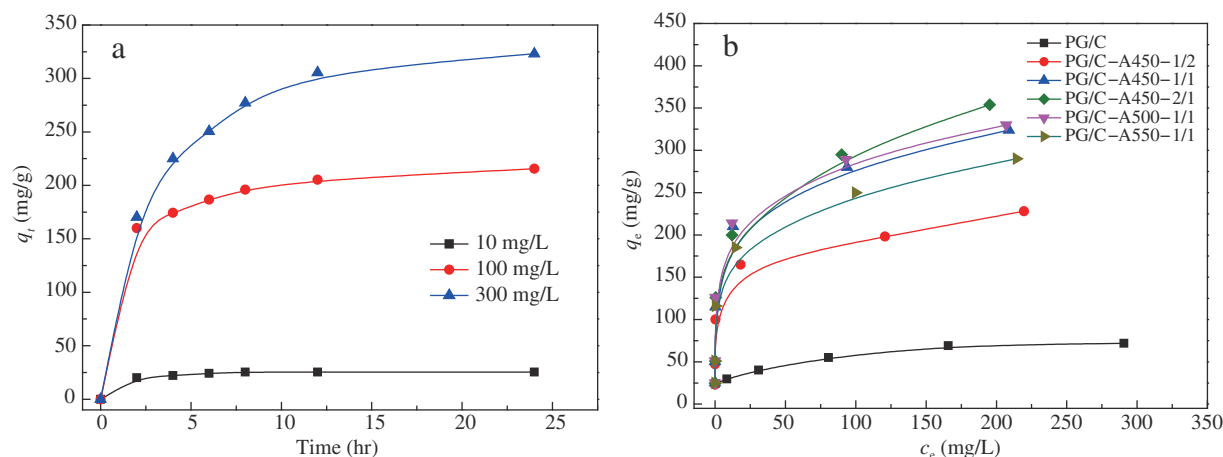


**Fig. 5 – (a) Dynamic adsorption of methylene blue (MB) on PG/C-A450-1/1 and (b) adsorption isotherms of MB on unactivated palygorskite/carbon (PG/C) and activated PG/C.**

**Table 3 – Comparison of the maximum adsorption capacity ( $q_m$ ) in different adsorbents.**

Adsorbent	Solid-liquid ratio (g/mL)	pH	T (°C)	Revolving speed (r/min)	t	$q_m$ (mg/g)	$S_{BET}$ (m <sup>2</sup> /g)	Reference
PG/C	0.0004	–	30	200	24 hr	89	106	This study
PG/C-A450-1/1	0.0004	–	30	200	24 hr	325	1201	This study
PG/C-A450-2/1	0.0004	–	30	200	24 hr	351	1044	This study
AC <sup>a</sup>	0.0004	–	30	200	24 hr	337	1441	This study
CAC <sup>b</sup>	0.0004	–	30	200	24 hr	318	927	This study
Ag NPs-AC	0.0004	6	25	350	15 min	71	–	Ghaedi et al. (2012)
AC	0.0005	6	25	–	5 hr	270	1688	Li et al. (2013)
GO	0.0005	6	25	–	5 hr	244	32	Li et al. (2013)
CNTs	0.0005	6	25	–	5 hr	189	177	Li et al. (2013)
GAL-AC	0.001	9	25	300	24 hr	780	2038	Benadjemia et al. (2011)
PK-AC	0.012	7	–	–	45 min	185	103	Ghaedi et al. (2013)
PFAC	0.001	–	30	120	–	382	1223	Foo and Hameed (2012)
CGAC180	0.001	6	25	300	24 hr	182	925	Reffas et al. (2010)

$q_m$ : the maximum adsorption capacity; T: temperature; t: time; AC: activated carbon; CAC: commercial activated carbon; GO: graphene oxide; GAL-AC: activated carbon from globe artichoke leaves; PK-AC: activated carbon from *Pistacia Khinjuk*; PFAC: activated carbon from oil palm fiber; CGAC180: activated carbon from coffee grounds.

<sup>a</sup> Activated carbon after PG/C removed PG template.

<sup>b</sup> Commercial activated carbon.

slightly lower than those of PG-450, which may be due to destruction of the crystal structure of PG encroached by ZnCl<sub>2</sub>, reflected by the disappearance of PG XRD peaks. The low adsorption capacity on PG-A450-1/1 also suggests that activation of PG using ZnCl<sub>2</sub> did not cause an obvious increase in the adsorption capacity of MB. Thus, the presence of ZnCl<sub>2</sub> influences the development of the pore structure of amorphous carbon on the PG surface. Activation of the carbon in PG/C directly resulted in increased BET surface area and adsorption capacity.

### 2.8. Dynamic mechanical analyzer (DMA) test

The compressive strength of the samples was tested as shown in Fig. 7. AC represents activated carbon obtained by removing PG from PG/C-A450-1/1 using HF acid, while CAC represents commercial activated carbon. For PG/C-A450-1/1, a short elastic deformation stage (compressive strain at 0%–3.5%)

was found. At this stage, the compressive stress and strain were proportional. With further increase in static force, the powder became denser and the strain changed sharply. The densification stage (5% compressive strain) of PG/C-A450-1/1 started earlier than that of the other two samples. In addition, the activated PG/C (PG/C-A450-1/1) presented higher compressive stress than the other two activated carbons (AC and CAC) under the same compressive strain, indicating better mechanical compressive strength. Usually, monolithic adsorbents are used in the methane adsorption and gas storage industry, due to their small interparticle space and high density (Jordá-Beneyto et al., 2008; Lozano-Castello et al., 2002; Molina-Sabio et al., 2003). This implies that activated carbon coated onto PG undoubtedly has potential advantages in the fabrication of massive monolithic adsorbents. The density of PG/C-A450-1/1 (0.72 g/cm<sup>3</sup>) was higher than that of AC (0.25 g/cm<sup>3</sup>) and CAC (0.58 g/cm<sup>3</sup>). The fact that PG/C-A450-1/1 has higher density suggests that separation of the adsorbent from the liquid can be easily achieved once the adsorbent is used in wastewater treatment.

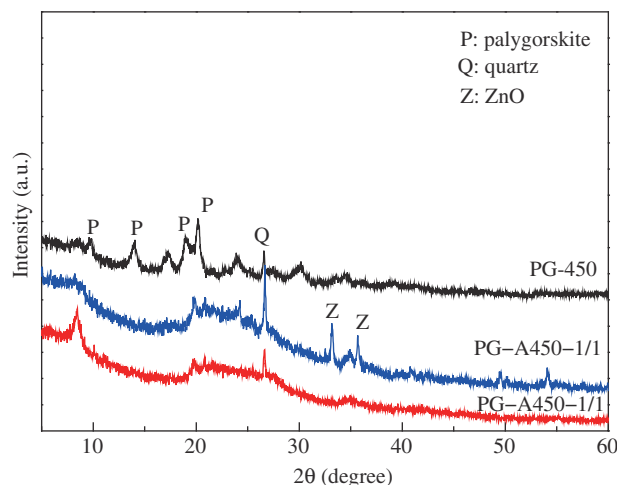


**Fig. 6 – XRD patterns of different samples with different treatments. PG-450 and PG-A450-1/1 refer to Section 2.7.**

### 3. Conclusions

An activated carbon coated on PG was prepared using ZnCl<sub>2</sub> as the activation agent and PG/C as the precursor. During the activation process, the PG fiber folded and collapsed

**Table 4 – Equilibrium adsorption capacity of methylene blue (MB) onto various samples.**

Sample	$q_e$ (mg/g)	$\eta$ (%)
PG/C	50	21
PG-450	70	28
PG-A450-1/1	68	27
PG/C-A450-1/1	220	87

$q_e$ : the adsorption capacity at equilibrium;  $\eta$ : the removal rate of MB.

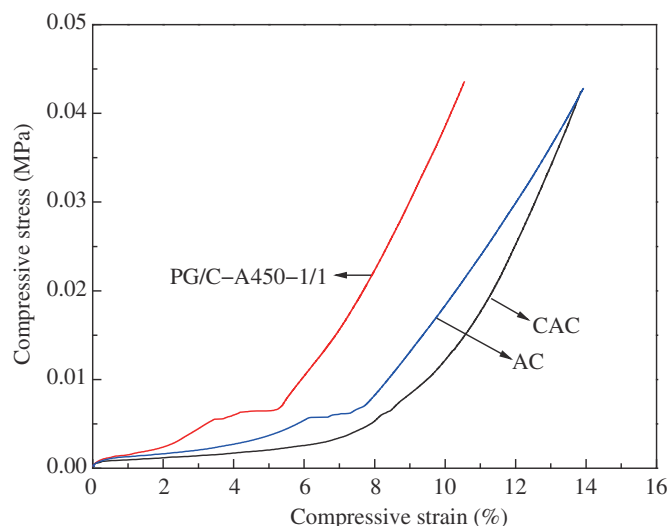


**Fig. 7 – Compressive stress versus compressive strain curves of various samples. AC: activated carbon obtained by removing PG from PG/C-A450-1/1 using HF acid; CAC: commercial activated carbon.**

while the surface carbon was developed and carbonized. The well-developed pore structure of carbon resulted in increased specific surface area and changes in surface chemistry. The C–H groups of PG/C disappeared and C=C groups were formed in the activated PG/C. The textural structure and surface chemistry of activated PG/C could be controlled by adjusting the activation conditions, such as activation temperature and impregnation ratio. The optimum activation condition was determined to be 1:1 impregnation ratio and 450°C activation temperature. In this condition, the BET surface area was the highest, with a value of 1201 m<sup>2</sup>/g. PG/C-A450-2/1, which had the largest external surface area and pore volume, exhibited the highest adsorption capacity ( $q_m$ ) for MB of 351 mg/g, which was far greater than that of untreated PG/C. The maximum adsorption capacity of MB onto activated carbon after being stripped of PG was also very high (337 mg/g). The mechanical compressive strength of activated-carbon-coated PG was better than that of activated carbon stripped from the template PG. This suggests that the activated PG/C has strong potential for use as a block adsorbent in the waste treatment industry.

### Acknowledgments

The authors are very grateful for the help from Professor Yanwei Ding of Thermal Analysis Laboratory, Instruments' Center for Physical Science, University of Science and Technology of China (USTC), Hefei, Anhui, China for porosity analysis and DMA testing of the samples. This work was financially supported by the National Natural Science Foundation of China (No. 51002042, No. 40902020 and No. 51072044), the Fundamental Research Funds for the Central Universities (No. 2013HGQC0015), Scientific Research Foundation for the Returned Scholars from Ministry of Education of China (No. 2013JYLH0774) and Project from Ministry of Science and Technology of Anhui Province (No. J2014AKKJ0002).

### Appendix A. Supplementary data

Supplementary data to this article can be found online at <http://dx.doi.org/10.1016/j.jes.2015.01.014>.

### REFERENCES

- Altenor, S., Carene, B., Emmanuel, E., Lambert, J., Ehrhardt, J.J., Gaspard, S., 2009. Adsorption studies of methylene blue and phenol onto vetiver roots activated carbon prepared by chemical activation. *J. Hazard. Mater.* 165 (1–3), 1029–1039.
- Banaś, D., Kubala-Kukuś, A., Braziewicz, J., Majewska, U., Pajek, M., Wudarczyk-Močko, J., et al., 2013. Study of properties of chemically modified samples of halloysite mineral with X-ray fluorescence and X-ray powder diffraction methods. *Radiat. Phys. Chem.* 93, 129–134.
- Benadjemia, M., Millière, L., Reinert, L., Benderdouche, N., Duclaux, L., 2011. Preparation characterization and methylene blue adsorption of phosphoric acid activated carbons from globe artichoke leaves. *Fuel Process. Technol.* 92 (6), 1203–1212.
- Chang, B.B., Shi, W.W., Guan, D.X., Wang, Y.L., Zhou, B.C., Dong, X.P., 2014. Hollow porous carbon sphere prepared by a facile activation method and its rapid phenol removal. *Mater. Lett.* 126, 13–16.
- Chen, H., Zhao, J., Zhong, A.G., Jin, Y.X., 2011. Removal capacity and adsorption mechanism of heat-treated palygorskite clay for methylene blue. *Chem. Eng. J.* 174 (1), 143–150.
- Chiu, K.L., Ng, D.H.L., 2012. Synthesis and characterization of cotton-made activated carbon fiber and its adsorption of methylene blue in water treatment. *Biomass Bioenergy* 46, 102–110.
- Ding, L.L., Zou, B., Li, Y.N., Liu, H.Q., Wang, Z.C., Zhao, C., et al., 2013. The production of hydrochar-based hierarchical porous carbons for use as electrochemical supercapacitor electrode materials. *Colloids Surf. A* 423, 104–111.
- Donald, J., Ohtsuka, Y., Xu, C., 2011. Effects of activation agents and intrinsic minerals on pore development in activated carbons derived from a Canadian peat. *Mater. Lett.* 65 (4), 744–747.

- Foo, K.Y., Hameed, B.H., 2012. Adsorption characteristics of industrial solid waste derived activated carbon prepared by microwave heating for methylene blue. *Fuel Process. Technol.* 99, 103–109.
- Frost, R.L., Ding, Z., 2003. Controlled rate thermal analysis and differential scanning calorimetry of sepiolites and palygorskites. *Thermochim. Acta* 397 (1–2), 119–128.
- Ghaedi, M., Heidarpour, S., Kokhdan, S.N., Sahraied, R., Daneshfar, A., Brazesh, B., 2012. Comparison of silver and palladium nanoparticles loaded on activated carbon for efficient removal of methylene blue: kinetic and isotherm study of removal process. *Powder Technol.* 228, 18–25.
- Ghaedi, M., Ghaedi, A.M., Abdi, F., Roosta, M., Vafaei, A., Asghari, A., 2013. Principal component analysis—adaptive neuro-fuzzy inference system modeling and genetic algorithm optimization of adsorption of methylene blue by activated carbon derived from *Pistacia Khinjuk*. *Ecotoxicol. Environ. Saf.* 96, 110–117.
- Guo, Y.P., Rockstraw, D.A., 2006. Physical and chemical properties of carbons synthesized from xylan, cellulose, and Kraft lignin by  $H_3PO_4$  activation. *Carbon* 44 (8), 1464–1475.
- Hao, W.M., Björkman, E., Lilliestråle, M., Hedin, N., 2013. Activated carbons prepared from hydrothermally carbonized waste biomass used as adsorbents for  $CO_2$ . *Appl. Energy* 112, 526–532.
- Hayashi, J., Kazehaya, A., Muroyama, K., Watkinson, A.P., 2000. Preparation of activated carbon from lignin by chemical activation. *Carbon* 38 (13), 1837–1878.
- Jordá-Beneyto, M., Lozano-Castello, D., Suárez-García, F., Cazorla-Amorós, D., Linares-Solano, A., 2008. Advanced activated carbon monoliths and activated carbons for hydrogen storage. *Microporous Mesoporous Mater.* 112 (1–3), 235–242.
- Juang, R.S., Wu, F.C., Tseng, R.L., 2000. Mechanism of adsorption of dyes and phenols from water using activated carbons prepared from plum kernels. *J. Colloid Interface Sci.* 227 (2), 437–444.
- Khezami, L., Chetouani, A., Taouk, B., Capart, R., 2005. Production and characterization of activated carbon from wood components in powder: cellulose, lignin, xylan. *Powder Technol.* 157 (1–3), 48–56.
- Kuang, W.X., Facey, G.A., Detellier, C., 2004. Dehydration and rehydration of palygorskite and the influence of water on the nanoporous. *Clays Clay Minerals* 52 (5), 635–642.
- Li, M., Li, W., Liu, S.X., 2011. Hydrothermal synthesis, characterization, and KOH activation of carbon spheres from glucose. *Carbohydr. Res.* 346 (8), 999–1001.
- Li, Y.H., Du, Q.J., Liu, T.H., Peng, X.J., Wang, J.J., Sun, J.K., et al., 2013. Comparative study of methylene blue dye adsorption onto activated carbon, graphene oxide, and carbon nanotubes. *Chem. Eng. Res. Des.* 91 (2), 361–368.
- Liu, T.H., Li, Y.H., Du, Q.J., Sun, J.K., Jiao, Y.Q., Yang, G.M., et al., 2012. Adsorption of methylene blue from aqueous solution by graphene. *Colloids Surf. B* 90, 197–203.
- Liu, Y.S., Cai, Q., Li, H.D., Zhang, J.M., 2013. Fabrication and characterization of mesoporous carbon nanosheets using halloysite nanotubes and polypyrrole via a template-like method. *J. Appl. Polym. Sci.* 128 (1), 517–522.
- Lozano-Castello, D., Cazorla-Amorós, D., Linares-Solano, A., Quinn, D.F., 2002. Activated carbon monoliths for methane storage: influence of binder. *Carbon* 40 (15), 2817–2825.
- Miao, Q.Q., Tang, Y.M., Xu, J., Liu, X.P., Xiao, L., Chen, Q.H., 2013. Activated carbon prepared from soybean straw for phenol adsorption. *J. Taiwan Inst. Chem. Eng.* 44 (3), 458–465.
- Mohanty, K., Das, D., Biswas, M.N., 2005. Adsorption of phenol from aqueous solutions using activated carbons prepared from *Tectonagrandis* sawdust by  $ZnCl_2$  activation. *Chem. Eng. J.* 115 (1–2), 121–131.
- Molina-Sabio, M., Almansa, C., Rodríguez-Reinoso, F., 2003. Phosphoric acid activated carbon discs for methane adsorption. *Carbon* 41 (11), 2113–2119.
- Nakagawa, Y., Molina-Sabio, M., Rodríguez-Reinoso, F., 2007. Modification of the porous structure along the preparation of activated carbon monoliths with  $H_3PO_4$  and  $ZnCl_2$ . *Microporous Mesoporous Mater.* 103 (1–3), 29–34.
- Reffas, A., Bernardet, V., David, B., Reinert, L., Lehocine, M.B., Dubois, M., et al., 2010. Carbons prepared from coffee grounds by  $H_3PO_4$  activation: characterization and adsorption of methylene blue and Nylosan Red N-2RBL. *J. Hazard. Mater.* 175 (1–3), 779–788.
- Regmi, P., Luis, J., Moscoso, G., Kumar, S., Cao, X.Y., Mao, J.D., et al., 2012. Removal of copper and cadmium from aqueous solution using switch grass biochar produced via hydrothermal carbonization process. *J. Environ. Manag.* 109, 61–69.
- Román, S., Nabais, J.M.V., Ledesma, B., González, J.F., Laginhas, C., Titirici, M.M., 2013. Production of low-cost adsorbents with tunable surface chemistry by conjunction of hydrothermal carbonization and activation processes. *Microporous Mesoporous Mater.* 165, 127–133.
- Romero-Anaya, A.J., Ouzzine, M., Lillo-Ródenas, M.A., Linares-Solano, A., 2014. Spherical carbons: synthesis, characterization and activation processes. *Carbon* 68, 296–307.
- Saka, C., 2012. BET, TG-DTG, FT-IR, SEM, iodine number analysis and preparation of activated carbon from acorn shell by chemical activation with  $ZnCl_2$ . *J. Anal. Appl. Pyrolysis* 95, 21–24.
- Sing, K.S.W., Everett, D.H., Haul, R.A.W., Moscou, L., Pierotti, R.A., Rouquerol, J., et al., 1985. Reporting physisorption data for gas/solid systems with special reference to the determination of surface area and porosity. *Pure Appl. Chem.* 57, 603–619.
- Theydan, S.K., Ahmed, M.J., 2012. Optimization of preparation conditions for activated carbons from date stones using response surface methodology. *Powder Technol.* 224, 101–108.
- Uçar, S., Erdem, M., Tay, T., Karagöz, S., 2009. Preparation and characterization of activated carbon produced from pomegranate seeds by  $ZnCl_2$  activation. *Appl. Surf. Sci.* 255 (21), 8890–8896.
- Wang, L.L., Guo, Y.P., Zou, B., Rong, C.G., Ma, X.Y., Qu, Y.N., et al., 2011. High surface area porous carbons prepared from hydrochars by phosphoric acid activation. *Bioresour. Technol.* 102 (2), 1947–1950.
- Williams, P.T., Reed, A.R., 2006. Development of activated carbon pore structure via physical and chemical activation of biomass fibre waste. *Biomass Bioenergy* 30 (2), 144–152.
- Wu, X.P., Zhu, W.Y., Zhang, X.L., Chen, T.H., Frost, R.L., 2011. Catalytic deposition of nanocarbon onto palygorskite and its adsorption of phenol. *Appl. Clay Sci.* 52 (4), 400–406.
- Wu, X.P., Liu, C., Zhang, L., Cheng, L.P., Zhang, X.L., 2013. Effect of the hydrothermally treatment on the palygorskite structures. *Adv. Mater. Res.* 726–731, 560–564.
- Wu, X.P., Gao, P., Zhang, X.L., Jin, G.P., Xu, Y.Q., Wu, Y.C., 2014a. Synthesis of clay/carbon adsorbent through hydrothermal carbonization of cellulose on palygorskite. *Appl. Clay Sci.* 95, 60–66.
- Wu, X.P., Xu, Y.Q., Zhang, X.L., Wu, Y.C., Gao, P., 2014b. Adsorption of low-concentration methylene blue onto palygorskite/carbon nanocomposite. *New Carbon Mater.* 29 (5), 1–8.
- Yavuz, R., Akyildiz, H., Karatepe, N., Çetinkaya, E., 2010. Influence of preparation conditions on porous structures of olive stone activated by  $H_3PO_4$ . *Fuel Process. Technol.* 91 (1), 80–87.
- Yue, Z.R., Wang, J.W., Economy, J., 2013. Pore control of  $ZnCl_2$ -activated cellulose on fiberglass mats for removal of humic acid from water. *Mater. Lett.* 90, 8–10.
- Zhao, S., Li, X.Y., Wang, C.Y., Chen, M.M., 2012. Preparation of bowl-like and eggshell-like hollow carbon microspheres from potato starch. *Mater. Lett.* 70, 54–56.
- Zhou, F.J., Bian, W.B., Yu, H., Zhong, Y., Mao, Z.P., 2014. Molecular simulation of the aggregation behaviors of high-concentration reactive dyes in aqueous solution. *Text. Dyeing Finish. J.* 36 (5), 9–15 (In Chinese).
- Zhu, Z.L., Li, A.M., Yan, L., Liu, F.Q., Zhang, Q.X., 2007. Preparation and characterization of highly mesoporous spherical activated carbons from divinylbenzene-derived polymer by  $ZnCl_2$  activation. *J. Colloid Interface Sci.* 316 (2), 628–634.